Target Detection for Distributed MIMO Radar with Non-Orthogonal Waveforms in Cluttered Environments

Cengcang Zeng, *Student Member, IEEE*, Fangzhou Wang, *Member, IEEE*, Hongbin Li, *Fellow, IEEE,* and Mark A. Govoni, *Senior Member, IEEE*

***Abstract*—Orthogonal radar waveforms originating from spatially distributed transmitters (TXs) usually arrive at a receiver (RX) in non-orthogonal forms, as they propagate through different paths with distinct delays and Doppler frequencies in distributed multi-input multi-output (MIMO) radar. Non-orthogonal waveforms complicate the composition of the target and clutter returns, making it more challenging to separate one from the other. In this paper, we consider joint target detection and clutter mitigation in distributed MIMO radar. We first present a general signal model for distributed MIMO radar in cluttered environments. Next, we propose three families of detection solutions, including non-coherent detectors that require no phase estimation and are relatively simple to implement, coherent detectors that offer enhanced detection performance given accurate phase information, and hybrid detectors that are a compromise of the former two, requiring only local phase coherence but no explicit phase estimation. In addition, approximate solutions are proposed in each category with further complexity reduction, using high clutter-to-noise (CNR) approximation or convex relaxation. Simulation results are presented to demonstrate the performance of the proposed detectors, which outperform their earlier counterparts that neglect the presence of clutter.**

***Index Terms*—Distributed MIMO radar, target detection, clutter mitigation, non-orthogonal waveforms**

I. Introduction

Distributed multi-input multi-output (MIMO) radar, which can detect and track targets of interest by employing widely separated antennas with multiple waveforms, has received significant attention in recent years [1]. Unlike its counterpart, co-located MIMO radar with closely spaced antennas, distributed MIMO radar can probe a target from different aspect angles and exploit the spatial or geometric diversity to enhance radar performance. Some recent works on distributed MIMO radar include diversity gain analysis [2], [3], direction finding [4], target detection [5]–[9], target localization using various techniques (e.g., sparse modeling [10], weighted least squares algorithm [11], and Lagrange programming neural network approach [12]), waveform/code design [13], [14], optimal power allocation [15] and antenna configuration [16]–[18], phase errors [19] and registration errors [20], spectral coexistence of distributed MIMO radar and multi-user MIMO communication systems [21], and development of a distributed dual-function radar-communication MIMO system [22].

Most prior studies on MIMO radar assume that the waveforms emitted from different transmitters (TXs) are orthogonal and that orthogonality is preserved at the receivers (RXs). As such, different waveforms as well as the information carried by them can be perfectly separated at the receivers by using a set of matched filters (MFs), one for each waveform. However, orthogonality cannot be maintained in practice for all Doppler and delay pairs [23]–[25]. The problem becomes more critical in distributed MIMO radar, where radar echoes are inherently *dispersive in time and frequency*. Specifically, the propagation delays and, respectively, Doppler frequencies for the same moving target are in general different for different TX-RX pairs, due to the different bi-static geometries associated with them. This would cause orthogonal waveforms on transmit to become non-orthogonal at the RXs. Therefore, it is important to study the effect of non-orthogonal waveforms on the performance of MIMO radar. Direction-of-arrival (DOA) estimation with co-located MIMO radar and non-orthogonal waveforms was studied in [26]–[28]. Target detection in distributed MIMO radar with imperfect waveform separation was considered in [29], [30]. In particular, [29] modeled the cross-correlation among the signals received from different transmitters as deterministic unknowns and examined the sensitivity of target detection against the cross-correlation strength. In [30], a distributed generalized likelihood ratio test (GLRT) was developed by treating the target residual due to imperfect waveform separation as a statistic quantity with an unknown covariance matrix. Meanwhile, [8] developed a general framework for target detection in distributed MIMO radar with non-orthogonal waveforms in clutter-free environments, which also incorporates effects of timing, frequency, and phase errors among different TXs and RXs.

Another major challenge with distributed MIMO radar is clutter mitigation. Due to the multi-static configuration of distributed MIMO radar, the clutter is inherently *non-homogeneous* and exhibits distinct characteristics across different TX-RX pairs and different range resolution cells [31]. To address this problem, prior studies considered various techniques to model, estimate, and reject the non-homogeneous clutter in distributed MIMO radar, by using a discrete/subspace

This work was supported in part by the Army Research Office under Cooperative Agreement Number W911NF-19-2-0234 and the National Science Foundation under grants ECCS-1923739 and ECCS-2212940.

C. Zeng, F. Wang, and H. Li are with the Department of Electrical and Computer Engineering, Stevens Institute of Technology, Hoboken, NJ 07030 USA (e-mail:czeng2@stevens.edu; fwang11@stevens.edu; hli@stevens.edu).

M. A. Govoni is with Army Research Laboratory, Aberdeen Proving Ground, MD 21005 USA.

Corresponding author: H. Li.

clutter model [31]–[36], a parametric autoregressive approach [31], [37], a compound Gaussian clutter model [38]–[40], and a Bayesian scheme based on a complex Wishart or complex inverse Wishart prior [41], [42], among others. Most of these works, however, assume the radar waveforms are orthogonal, in which case the clutter becomes independent of the radar waveforms due to MF processing. With non-orthogonal waveforms, the problem is more challenging. This is because a clutter echo from each clutter scatterer is a superposition of the radar waveforms emitted from different TXs, which arrive at a RX with different delays and Doppler shifts. After MF processing, the clutter consists of both an *auto term*, which refers to the auto correlation of the radar waveform the MF is matched to, and multiple *cross terms*, which are the cross correlations between the desired and other radar waveforms. As a result, the clutter in distributed MIMO radar is in general waveform dependent and more difficult to characterize/mitigate.

In this paper, we consider joint moving target detection and clutter mitigation in distributed MIMO radar with non-orthogonal waveforms. We first derive a general signal model for distributed MIMO radar with non-orthogonal waveforms in cluttered environments, and then examine the covariance structure of the clutter signal comprising both auto and cross terms. The moving target detection problem is solved by using the GLRT framework, which results in three categories of detectors, covering non-coherent, coherent, and hybrid detection, respectively. The non-coherent approach, which requires no phase estimation, is the simplest among the three for implementation, while the coherent approach is the opposite. The hybrid approach, which needs local phase coherence and performs non-coherent integration across different TX-RX pairs, is a compromise between the former two. Meanwhile, it turns out that the maximum likelihood estimates (MLEs) of the clutter powers cannot be obtained in closed form, we develop suboptimal clutter power estimators, which are obtained based on either a high clutter-to-noise ratio (CNR) approximation or convex relaxation, to reduce the computational complexity of the GLRT. Extensive simulation results show that all proposed detectors significantly outperform their counterparts in [8] that neglects the clutter.

The remainder is organized as follows. A general signal model for distributed MIMO radar with non-orthogonal waveforms in cluttered environments and the moving target detection problem are presented in Section II. The proposed non-coherent, coherent, and hybrid detectors are detailed in Sections III, IV and V, respectively. Section VI contains numerical results, followed by conclusions in Section VII.

Notations: We use boldface symbols for vectors (lower case) and matrices (upper case). $(\cdot)^T$ denotes the transpose and $(\cdot)^H$ the conjugate transpose. $\|\cdot\|$ denotes the determinant of a matrix. $\mathbb{E}\{\cdot\}$ represents the statistical expectation. $\mathcal{CN}(\mathbf{u},\mathbf{\Sigma})$ denotes the complex Gaussian distribution with mean $\mathbf{u}$ and covariance matrix $\mathbf{\Sigma}$. $[\mathbf{X}]_{m,n}$ indicates the (m,n)-th element of the matrix $\mathbf{X}$ while $[\mathbf{x}]_m$ denotes the m-th element of the vector $\mathbf{x}$.

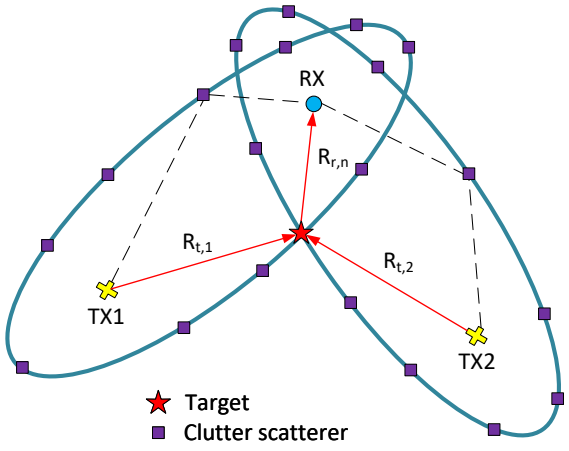

Figure 1. A distributed MIMO radar with $M = 2$ TXs and $N = 1$ RX. Each TX/RX pair and the target specifies an *isorange* which is an ellipse with foci at the TX and RX. The RX receives returns from the target and all clutter scatterers on the *isorange*.

II. Signal Model and Problem Formulation

In this section, we first extend the signal model of [8] by considering the target detection problem for a distributed MIMO radar with non-orthogonal waveforms in cluttered environments. Then, we examine the covariance structure of the clutter signal. Finally, we formulate the moving target detection problem by explicitly accounting for the signal model with clutter.

A. Signal Model

Consider a distributed MIMO radar, which is equipped with M TXs and N RXs. The system probes the environment using M distinct waveforms, one from each TX, and pulsed transmission. Each coherent processing interval (CPI) consists of K periodic pulses. Suppose there is a moving target located at a distance $R_{\mathrm{t},m}$ to the m-th TX and a distance $R_{\mathrm{r},n}$ to the n-th RX. The range sum $R_{\mathrm{t},m} + R_{\mathrm{r},n}$ specifies an *isorange*, which is an ellipse with foci at the TX and RX [31], as shown in Fig.1. Suppose there are $L_{m,n}$ clutter scatterers on the *isorange* of the (m,n)-th TX-RX pair. Then, the noise-free received signal at the RX can be expressed as (cf. [8]):

$$s_n(t) = \sum_{m=1}^{M} \alpha \xi_{mn} u_m(t-\tau_{mn}) e^{\jmath\psi_{mn}} e^{\jmath 2\pi(f_c+f_{mn})(t-\tau_{mn})} + \sum_{m=1}^{M}\sum_{l=1}^{L_{mn}} \widetilde{\alpha}_{mnl}\widetilde{\xi}_{mnl} u_m(t-\tau_{mn}) e^{\jmath\psi_{mn}} e^{\jmath 2\pi(f_c+\widetilde{f}_{mnl})(t-\tau_{mn})}, \tag{1}$$

where

- α and $\widetilde{\alpha}_{mnl}$ denote the radar cross section (RCS) of the target and, respectively, the (m,n,l)-th clutter scatterer.
- ξ_{mn} and $\widetilde{\xi}_{mnl}$ are the channel coefficients, which lump the path loss and antenna gains [8], associated with the (m,n)-th TX-RX pair of the target path and the (m,n,l)-th scatterer path, respectively.

- $u_m(t) = \sum_{k=0}^{K-1} p_m(t - kT_{\rm s})$ is the baseband transmitted signal which comprises K repetitions of the pulse waveform $p_m(t)$ with T_s being the pulse repetition interval.
- ψ_{mn} denotes the phase offset between the oscillators at the m-th TX and the n-th RX.
- $\tau_{mn} = (R_{{\rm t},m} + R_{{\rm r},n})/c$ is the propagation delay associated with the (m,n)-th TX-RX pair and c is the speed of light.
- f_c is the carrier frequency, while f_{mn} and $\widetilde{f}_{mnl}$ denote the Doppler frequency of the target and the (m,n,l)-th clutter scatterer.

After down conversion, the received signal passes through M matched filters (MFs) with impulse response $g_m(t) = p_m^*(-t)e^{\jmath 2\pi f_{mn}t}$, $m = 1,\ldots,M$. Then, the output of the m-th MF at the n-th RX $x_{mn}(t)$ can be written as:

$$\begin{aligned} x_{mn}(t) &= \sum_{\bar{m}=1}^{M} \alpha \xi_{\bar{m}n} e^{\jmath\psi_{mn}} e^{-\jmath 2\pi f_{\rm c}\tau_{\bar{m}n}} e^{\jmath 2\pi f_{mn}(t-\tau_{\bar{m}n})} \\ &\times \sum_{k=0}^{K-1} \chi_{m\bar{m}}(t - \tau_{\bar{m}n} - kT_{\rm s}, f_{\bar{m}n} - f_{mn}) e^{\jmath 2\pi k T_{\rm s}(f_{\bar{m}n} - f_{mn})} \\ &+ \sum_{\bar{m}=1}^{M} \sum_{l=1}^{L_{\bar{m}n}} \widetilde{\alpha}_{\bar{m}nl} \widetilde{\xi}_{\bar{m}nl} e^{\jmath\psi_{mn}} e^{-\jmath 2\pi f_{\rm c}\tau_{\bar{m}n}} e^{\jmath 2\pi f_{mn}(t-\tau_{\bar{m}n})} \\ &\times \sum_{k=0}^{K-1} \chi_{m\bar{m}}(t - \tau_{\bar{m}n} - kT_{\rm s}, \widetilde{f}_{\bar{m}nl} - f_{mn}) e^{\jmath 2\pi k T_{\rm s}(\widetilde{f}_{\bar{m}nl} - f_{mn})}, \end{aligned} \tag{2}$$

where $\chi_{m\bar{m}}(v,f)$ is the cross ambiguity function (CAF) defined as [8]

$$\chi_{m\bar{m}}(\nu, f) = \int p_m(\mu) p_{\bar{m}}^*(\mu - \nu) e^{\jmath 2\pi f \mu} d\mu. \tag{3}$$

The continuous-time MF output is sampled at the pulse rate, i.e., $t = \tau_{mn} + kT_s$, $k = 0,\cdots,K-1$, which yields:

$$\begin{aligned} x_{mn}(k) &= \sum_{\bar{m}=1}^{M} \alpha \xi_{\bar{m}n} e^{-\jmath 2\pi f_{\rm c}\tau_{\bar{m}n}} e^{\jmath 2\pi k T_{\rm s} f_{\bar{m}n}} e^{\jmath 2\pi f_{mn}(\tau_{mn} - \tau_{\bar{m}n})} \\ &\times e^{\jmath\psi_{mn}} \chi_{m\bar{m}}(\tau_{mn} - \tau_{\bar{m}n}, f_{\bar{m}n} - f_{mn}) + \sum_{\bar{m}=1}^{M} \sum_{l=1}^{L_{\bar{m}n}} \widetilde{\alpha}_{\bar{m}nl} \widetilde{\xi}_{\bar{m}nl} \\ &\times e^{-\jmath 2\pi f_{\rm c}\tau_{\bar{m}n}} e^{\jmath 2\pi k T_{\rm s} \widetilde{f}_{\bar{m}nl}} e^{\jmath 2\pi f_{mn}(\tau_{mn} - \tau_{\bar{m}n})} e^{\jmath\psi_{mn}} \\ &\times \chi_{m\bar{m}}(\tau_{mn} - \tau_{\bar{m}n}, f_{\bar{m}nl} - f_{mn}), \\ & m = 1,\ldots,M;\ n = 1,\ldots,N;\ k = 0,\ldots,K-1. \end{aligned} \tag{4}$$

Note that the output of the target signal consists of M components, i.e., $\bar{m} = m$ is the *auto term* that is the MF output matched to the m-th transmitted waveform and the other $M-1$ components are the *cross terms* that are the MF outputs matched to the rest $M-1$ waveforms. The clutter output has a similar composition. It can be seen that when the M waveforms are orthogonal across time and frequency, i.e., $\chi_{m\bar{m}}(\cdot,\cdot) = 0$, for $m \neq \bar{m}$, the $M-1$ cross terms vanish. However, maintaining such strict orthogonality in distributed MIMO radar is impossible [23]. Thus, the cross terms become non-negligible and need to be accounted for.

Remark: While the derivation of the model (4) appears to suggest that we need prior estimates of the target delays and Doppler frequencies, which are *unnecessary*. In practice, the radar receiver divides the uncertainty region of the target location and velocity into many location-velocity cells, which are similar to the range-Doppler bins in conventional monostatic radar. The radar scans each cell one by one, each of which corresponds to a set of known delays and Doppler frequencies for each TX-RX pair. The receiver uses a set of MFs matched to these delays and Dopplers. It should be noted that (4) describes the observed signal only for the cell that contains a target. For non-target cells, the measurements comprise only clutter and noise. The measurements for target and non-target cells are described by the hypothesis testing data model in (13).

Next, we stack the K slow-time samples and form $\mathbf{x}_{mn} = [x_{mn}(0),\cdots,x_{mn}(K-1)]^T$:

$$\mathbf{x}_{mn} = \alpha \mathbf{S}_n \mathbf{h}_{mn} + \sum_{\bar{m}=1}^{M} \widetilde{\mathbf{S}}_{\bar{m}n} {\rm diag}(\widetilde{\mathbf{h}}_{m\bar{m}n}) \widetilde{\boldsymbol{\alpha}}_{\bar{m}n}, \tag{5}$$

where

- $\mathbf{S}_n = [\mathbf{s}(f_{1n}),\cdots,\mathbf{s}(f_{Mn})]$ and $\widetilde{\mathbf{S}}_{\bar{m}n} = [\mathbf{s}(\widetilde{f}_{\bar{m}n1}),\cdots,\mathbf{s}(\widetilde{f}_{\bar{m}nL_{\bar{m}n}})]$ with $\mathbf{s}(f) = [1, e^{\jmath 2\pi T_{\rm s} f},\ldots,e^{\jmath 2\pi (K-1)T_{\rm s} f}]^T$.
- $\mathbf{h}_{mn} \in \mathbb{C}^{M\times 1}$ is the target channel vector with the $\bar{m}$-th element given by $[\mathbf{h}_{mn}]_{\bar{m}} = \xi_{\bar{m}n} e^{-\jmath 2\pi f_{\rm c}\tau_{\bar{m}n}} e^{\jmath 2\pi f_{mn}(\tau_{mn} - \tau_{\bar{m}n})} e^{\jmath\psi_{mn}} \chi_{m\bar{m}}(\tau_{mn} - \tau_{\bar{m}n}, f_{\bar{m}n} - f_{mn})$.
- $\widetilde{\mathbf{h}}_{m\bar{m}n} \in \mathbb{C}^{L_{\bar{m}n}\times 1}$ is the clutter channel vector with the l-th element given by $[\widetilde{\mathbf{h}}_{m\bar{m}n}]_l = \widetilde{\xi}_{\bar{m}nl} e^{-\jmath 2\pi f_{\rm c}\tau_{\bar{m}n}} e^{\jmath 2\pi f_{mn}(\tau_{mn} - \tau_{\bar{m}n})} e^{\jmath\psi_{mn}} \chi_{m\bar{m}}(\tau_{mn} - \tau_{\bar{m}n}, f_{\bar{m}nl} - f_{mn})$.
- $\widetilde{\boldsymbol{\alpha}}_{\bar{m}n} \in \mathbb{C}^{L_{\bar{m}n}\times 1}$ is the clutter RCS vector with the l-th element given by $[\widetilde{\boldsymbol{\alpha}}_{\bar{m}n}]_l = \widetilde{\alpha}_{\bar{m}nl}$.

B. Clutter Covariance Matrix

Since the clutter components contain reflections from unwanted stationary and slow moving objects (e.g., wind, rain, wave, etc.) within the considered test cell, their velocities and sizes are usually unknown. We assume that the clutter Doppler frequencies $\widetilde{f}_{\bar{m}nl}$ and reflection amplitudes $\alpha_{\bar{m}nl}$ are independent random variables. Specifically, $\widetilde{f}_{\bar{m}nl}$ are uniformly distributed in an interval of $[-\Delta_f, \Delta_f]$, where Δ_f denotes the maximum Doppler frequency, and $\widetilde{\alpha}_{\bar{m}nl}$ are Gaussian random variables with zero mean and variance $\sigma^2_{\bar{m}nl}$. Then, the $K \times K$ clutter covariance matrix can be expressed as

$$\begin{aligned} \boldsymbol{\Gamma}_{mn} &\overset{(a)}{=} \sum_{\bar{m}=1}^{M} \mathbb{E}\Big[\widetilde{\mathbf{S}}_{\bar{m}n} {\rm diag}(\widetilde{\mathbf{h}}_{m\bar{m}n}) \mathbb{E}\big[\widetilde{\boldsymbol{\alpha}}_{\bar{m}n} \widetilde{\boldsymbol{\alpha}}_{\bar{m}n}^H\big] {\rm diag}(\widetilde{\mathbf{h}}_{m\bar{m}n}^H) \widetilde{\mathbf{S}}_{\bar{m}n}^H\Big] \\ &= \sum_{\bar{m}=1}^{M} \mathbb{E}\big[\widetilde{\mathbf{S}}_{\bar{m}n} {\rm diag}(\widetilde{\mathbf{h}}_{m\bar{m}n}) \widetilde{\boldsymbol{\Lambda}}_{\bar{m}n} {\rm diag}(\widetilde{\mathbf{h}}_{m\bar{m}n}^H) \widetilde{\mathbf{S}}_{\bar{m}n}^H\big] \\ &\overset{(b)}{\approx} \sum_{\bar{m}=1}^{M} |\widetilde{\chi}_{m\bar{m}n}|^2 \mathbb{E}\big[\widetilde{\mathbf{S}}_{\bar{m}n} \widetilde{\boldsymbol{\Lambda}}_{\bar{m}n} \widetilde{\mathbf{S}}_{\bar{m}n}^H\big], \end{aligned} \tag{6}$$

where the outer $\mathbb{E}$ in (a) operates the expectation over the Doppler frequencies $f_{\bar{m}nl}$, while the inner $\mathbb{E}$ performs expec-

tation over the clutter RCS $\widetilde{\boldsymbol{\alpha}}_{\bar{m}nl}$. $\widetilde{\boldsymbol{\Lambda}}_{\bar{m}n}$ is an $L_{\bar{m}n} \times L_{\bar{m}n}$ diagonal matrix with diagonal elements given by

$$[\widetilde{\boldsymbol{\Lambda}}_{\bar{m}n}]_{l,l} = \widetilde{\xi}^2_{\bar{m}nl}\mathbb{E}[\widetilde{\alpha}_{\bar{m}nl}\widetilde{\alpha}^H_{\bar{m}nl}] = \sigma^2_{\bar{m}nl}\widetilde{\xi}^2_{\bar{m}nl}, \tag{7}$$

and

$$\widetilde{\chi}_{m\bar{m}n} = \chi_{m\bar{m}}(\tau_{mn} - \tau_{\bar{m}n}, 0). \tag{8}$$

Note that in (b) of (6), we used the approximation $\chi_{m\bar{m}}(\tau_{mn} - \tau_{\bar{m}n}, 0) \approx \chi_{m\bar{m}}(\tau_{mn} - \tau_{\bar{m}n}, f_{\bar{m}nl} - f_{mn})$ as the radar waveform is insensitive to small Doppler shift [43, p.15]. Then, the (k_1, k_2)-th element of $\boldsymbol{\Gamma}_{mn}$ can be further expressed as

$$\begin{aligned}
[\boldsymbol{\Gamma}_{mn}]_{k_1,k_2} &= \left[\sum_{\bar{m}=1}^{M} |\widetilde{\chi}_{m\bar{m}n}|^2 \mathbb{E}\big[\widetilde{\mathbf{S}}_{\bar{m}n}\widetilde{\boldsymbol{\Lambda}}_{\bar{m}n}\widetilde{\mathbf{S}}^H_{\bar{m}n}\big]\right]_{k_1,k_2} \\
&= \sum_{\bar{m}=1}^{M} |\widetilde{\chi}_{m\bar{m}n}|^2 \sum_{l=1}^{L_{\bar{m}n}} \sigma^2_{\bar{m}nl}\widetilde{\xi}^2_{\bar{m}nl}\mathbb{E}\big[e^{j2\pi(k_1-k_2)T_{\rm s}\widetilde{f}_{\bar{m}nl}}\big] \\
&= \sum_{\bar{m}=1}^{M} |\widetilde{\chi}_{m\bar{m}n}|^2 \sum_{l=1}^{L_{\bar{m}n}} \sigma^2_{\bar{m}nl}\widetilde{\xi}^2_{\bar{m}nl}\text{sinc}[2\pi\Delta_f(k_1-k_2)T_{\rm s}] \\
&= a_{mn}\text{sinc}[2\pi\Delta_f(k_1-k_2)T_{\rm s}],
\end{aligned} \tag{9}$$

where the clutter power a_{mn} is given by

$$a_{mn} = \sum_{\bar{m}=1}^{M} |\widetilde{\chi}_{m\bar{m}n}|^2 \sum_{l=1}^{L_{\bar{m}n}} \sigma^2_{\bar{m}nl}\widetilde{\xi}^2_{\bar{m}nl}. \tag{10}$$

Let

$$\begin{aligned}
[\boldsymbol{\Psi}]_{k_1,k_2} &= \text{sinc}[2\pi\Delta_f(k_1-k_2)T_{\rm s}], \\
& k_1, k_2 = 1, \cdots, K.
\end{aligned} \tag{11}$$

Then, the covariance matrix $\boldsymbol{\Gamma}_{mn}$ can be expressed as

$$\boldsymbol{\Gamma}_{mn} = a_{mn}\boldsymbol{\Psi}, \tag{12}$$

which consists of an unknown power coefficient a_{mn} and a covariance structure matrix $\boldsymbol{\Psi}$ that depends on the clutter Doppler bandwdith Δ_f.

C. Problem Statement

Let $\mathbf{y}_{mn}$ denote the noise-contaminated observation of $\mathbf{x}_{mn}$. The problem of interest is to detect the presence/absence of a moving target in the test cell using observations $\{\mathbf{y}_{mn}\}$. Specifically, the problem involves the following hypothesis testing:

$$\begin{aligned}
&\mathcal{H}_0 : \mathbf{y}_{mn} = \sum_{\bar{m}=1}^{M} \widetilde{\mathbf{S}}_{\bar{m}n}\text{diag}(\widetilde{\mathbf{h}}_{m\bar{m}n})\widetilde{\boldsymbol{\alpha}}_{\bar{m}n} + \mathbf{w}_{mn}, \\
&\mathcal{H}_1 : \mathbf{y}_{mn} = \alpha\mathbf{S}_n\mathbf{h}_{mn} + \sum_{\bar{m}=1}^{M} \widetilde{\mathbf{S}}_{\bar{m}n}\text{diag}(\widetilde{\mathbf{h}}_{m\bar{m}n})\widetilde{\boldsymbol{\alpha}}_{\bar{m}n} + \mathbf{w}_{mn}, \\
&\qquad m = 1, 2, \cdots, M,\ n = 1, 2, \cdots, N,
\end{aligned} \tag{13}$$

where $\mathbf{w}_{mn}$ denotes the white Gaussian noise with zero mean and covariance matrix $\sigma^2\mathbf{I}$, i.e., $\mathbf{w}_{mn} \sim \mathcal{CN}(\mathbf{0}, \sigma^2\mathbf{I})$, where σ^2 is the noise variance. The clutter is modeled as a Gaussian vector, which is independent of the noise, with zero mean and covariance matrix given by (12). It will be useful for later discussion to introduce the covariance matrix of both the clutter and noise:

$$\mathbf{R}(a_{mn}) \triangleq a_{mn}\boldsymbol{\Psi} + \sigma^2\mathbf{I}, \tag{14}$$

where the dependence on the clutter power coefficient a_{mn} is explicitly shown.

In the following sections, we address the detection problem by developing three categories of detectors, covering non-coherent, coherent, and hybrid detection, respectively. In all of our developments, it is assumed that the noise power σ^2, which can be determined by calibration prior to radar operation, is known.

III. Non-coherent detection in clutter

In this section, we first develop a non-coherent detector in clutter (NCDC) by using a GLRT framework that treats the target signal in (13) as an unknown quantity with no specific structure. It turns out that the MLE of the clutter power under the $\mathcal{H}_0$ hypothesis does not have a closed-form solution. To bypass a brute force search over the parameter space, two suboptimal clutter power estimators, which are based on a high CNR approximation and, respectively, a convex relaxation, are proposed to reduce the computational complexity of the GLRT.

A. NCDC

The detection problem can be solved by using a GLRT approach along with the MLEs of the unknown parameters. In the absence of phase coherence, it is generally impossible to estimate the individual components of the target signal $\alpha\mathbf{S}_n\mathbf{h}_{mn}$. Instead, we can estimate the target signal $\boldsymbol{\mu}_{mn} \triangleq \alpha\mathbf{S}_n\mathbf{h}_{mn}$ as an unstructured vector. Specifically, the GLRT is given by the likelihood ratio with the parameters replaced by their MLEs:

$$\frac{\max\limits_{\{\boldsymbol{\mu}_{mn}\},\{a_{mn}\}}\ p_1\big(\{\mathbf{y}_{mn}\}|\{\boldsymbol{\mu}_{mn}\},\{a_{mn}\}\big)}{\max\limits_{\{a_{mn}\}}\ p_0\big(\{\mathbf{y}_{mn}\}|\{a_{mn}\}\big)}, \tag{15}$$

where $p_1(\{\mathbf{y}_{mn}\}|\{\boldsymbol{\mu}_{mn}\},\{a_{mn}\})$ and $p_0(\{\mathbf{y}_{mn}\}|\{a_{mn}\})$ denote the likelihood functions under $\mathcal{H}_1$ and $\mathcal{H}_0$, respectively.

The MLEs of the parameters in (15) are discussed in Appendix I. It is shown there that the GLRT reduces to

$$T_{\text{NCDC}} = \sum_{m=1}^{M}\sum_{n=1}^{N} \big(\ln|\hat{\mathbf{R}}_0| + \mathbf{y}^H_{mn}\hat{\mathbf{R}}_0^{-1}\mathbf{y}_{mn}\big) \underset{\mathcal{H}_0}{\overset{\mathcal{H}_1}{\gtrless}} \gamma_{\text{NCDC}}, \tag{16}$$

where γ_{NCDC} denotes a test threshold and $\hat{\mathbf{R}}_0 = \mathbf{R}(\hat{a}_{mn,0})$, with $\hat{a}_{mn,0}$ denoting the MLE of the clutter under $\mathcal{H}_0$:

$$\hat{a}_{mn,0} = \arg\min_{a_{mn}}\ \ln|\mathbf{R}(a_{mn})| + \mathbf{y}^H_{mn}\mathbf{R}^{-1}(a_{mn})\mathbf{y}_{mn}, \tag{17}$$

which is non-convex and can be solved by a 1-dimensional (1-D) search over the non-negative real axis. In the next subsections, we propose two suboptimal solutions based on approximations to reduce the computational complexity.

The GLRT (16) is referred to as the NCDC detector, which involves whitening by the covariance matrix $\hat{\mathbf{R}}_0$ followed by energy integration. Note that $\hat{\mathbf{R}}_0$ is a real-valued covariance matrix. The above whitening and integration process does not utilize the phase information of the observations $\mathbf{y}_{mn}$. Hence, the NCDC is a non-coherent detector.

B. High CNR Approximation

Since the clutter is usually much stronger than the noise, i.e., $a_{mn} \gg \sigma^2$, we have $a_{mn}\mathbf{\Psi} + \sigma^2\mathbf{I} \approx a_{mn}(\mathbf{\Psi} + \sigma^2\mathbf{I})$. Then, the optimization problem in (17) can be approximated as

$$\hat{a}_{mn,0} \approx \arg \min_{a_{mn}} \ln\big(a_{mn}^K|\widetilde{\mathbf{R}}|\big) + \frac{1}{a_{mn}}\mathbf{y}_{mn}^H\widetilde{\mathbf{R}}^{-1}\mathbf{y}_{mn}, \quad (18)$$

where

$$\widetilde{\mathbf{R}} = \mathbf{\Psi} + \sigma^2\mathbf{I}. \quad (19)$$

The problem can be solved in closed-form with

$$\hat{a}_{mn,0} \approx \frac{1}{K}\mathbf{y}_{mn}^H\widetilde{\mathbf{R}}^{-1}\mathbf{y}_{mn}. \quad (20)$$

Substituting (20) into $p_0\big(\{\mathbf{y}_{mn}\}|\{a_{mn}\}\big)$, the likelihood function under $\mathcal{H}_0$ reduces to

$$p_0\big(\{\mathbf{y}_{mn}\}\big) = \prod_{m=1}^{M}\prod_{n=1}^{N}\frac{1}{(\mathbf{y}_{mn}^H\widetilde{\mathbf{R}}^{-1}\mathbf{y}_{mn})^K}. \quad (21)$$

As shown in Appendix I, the GLRT depends only on the likelihood function under $\mathcal{H}_0$. This leads to a new non-coherent detector in clutter with high CNR approximation (NCDC-A):

$$T_{\text{NCDC-A}} = \prod_{m=1}^{M}\prod_{n=1}^{N}\mathbf{y}_{mn}^H\widetilde{\mathbf{R}}^{-1}\mathbf{y}_{mn} \underset{\mathcal{H}_0}{\overset{\mathcal{H}_1}{\gtrless}} \gamma_{\text{NCDC-A}}, \quad (22)$$

which has an intuitive form of whitening followed by energy integration over all pulses and TX-RX pairs.

C. Convex Relaxation

The above approximation is valid only under high CNR. In the following, we transfer the non-convex optimization in (17) into a convex one by using majorization-minimization, which employs an iterative process to find the solution. Let $a_{mn}^{(l)}$ denote an estimate of a_{mn} obtained from the l-th iteration. Then, the concave term in (17), i.e., $\ln\big|\mathbf{R}(a_{mn}\big|$, can be upperbounded by using its first-order Taylor expansion as [44]

$$\begin{aligned}\ln\big|\mathbf{R}(a_{mn})\big| \leq& \text{tr}\big(\mathbf{R}^{-1}(a_{mn}^{(l)})\mathbf{\Psi}\big)(a_{mn} - a_{mn}^{(l)}) \\ &+ \ln\big|\mathbf{R}(a_{mn}^{(l)})\big|, \end{aligned} \quad (23)$$

where the equality is achieved at $a_{mn} = a_{mn}^{(l)}$.

Thus, during the $(\ell+1)$-st iteration, the non-convex problem is relaxed into the following convex optimization problem to obtain $a_{mn}^{(l+1)}$:

$$\min_{a_{mn}} \ \text{tr}\big(\mathbf{R}^{-1}(a_{mn}^{(l)})\mathbf{\Psi}\big)a_{mn} + \text{tr}\big(\mathbf{R}^{-1}(a_{mn})\mathbf{y}_{mn}\mathbf{y}_{mn}^H\big), \quad (24)$$

where the cost function is obtained by dropping the constant terms that are independent of a_{mn}. After convergence, (24) results in an approximate MLE of a_{mn} under $\mathcal{H}_0$. Then, we substitute it into (16). The resulting detector is referred to as the non-coherent detector in clutter with convex approximation (NCDC-CA).

IV. Coherent detection in clutter

In standard radar detection, the target location-velocity (range-Doppler) uncertainty region is divided into a finite number of test cells, and detection is performed on each cell one by one [45]. The target delays and Doppler frequencies associated with each test cell are known. For coherent detection, the radar receiver also keeps track of the phase offset ψ_{mn} between each TX-RX pair. As such, the receiver can form the target Doppler matrix $\mathbf{S}_n$ and channel vector $\mathbf{h}_{mn}$ [cf. (5)]. This leaves the target RCS α as the only unknown target parameter under $\mathcal{H}_1$, while the clutter power parameters a_{mn} remain as unknowns under both hypotheses. In view of the above discussion, a coherent detector in clutter (CDC) can be obtained by using the GLRT framework as

$$\frac{\max\limits_{\alpha,\{a_{mn}\}} \ p_1\big(\{\mathbf{y}_{mn}\}|\alpha,\{a_{mn}\}\big)}{\max\limits_{\{a_{mn}\}} \ p_0\big(\{\mathbf{y}_{mn}\}|\{a_{mn}\}\big)}, \quad (25)$$

where $p_1(\{\mathbf{y}_{mn}\}|\alpha,\{a_{mn}\})$ denotes the likelihood function under $\mathcal{H}_1$, while $p_0\big(\{\mathbf{y}_{mn}\}|\{a_{mn}\}\big)$ the likelihood function under $\mathcal{H}_0$ which is the same as in (15) for the NCDC. Thus, the MLE of a_{mn} under $\mathcal{H}_0$ is given by (17), which requires 1-D search.

The log likelihood function (LLF) $\ln\, p_1\big(\{\mathbf{y}_{mn}\}|\alpha,\{a_{mn}\}\big)$ is similar to (49), except that the mean $\boldsymbol{\mu}_{mn}$ is replaced by its structured version $\alpha\mathbf{S}_n\mathbf{h}_{mn}$. The MLEs of α and a_{mn} under $\mathcal{H}_1$ can be obtained in a sequential manner. Specifically, we first obtain the MLE of α by taking the derivative of the LLF with respect to (w.r.t.) α and setting it to zero, which gives

$$\hat{\alpha} = \big(\mathbf{z}_{mn}^H\mathbf{R}^{-1}(a_{mn})\mathbf{z}_{mn}\big)^{-1}\mathbf{z}_{mn}^H\mathbf{R}^{-1}(a_{mn})\mathbf{y}_{mn}, \quad (26)$$

where

$$\mathbf{z}_{mn} = \mathbf{S}_n\mathbf{h}_{mn}. \quad (27)$$

Substituting (26) back into the LLF yields

$$\begin{aligned} f_{\text{CDC}}(a_{mn}) =& -\ln|\mathbf{R}(a_{mn})| - \mathbf{y}_{mn}^H\mathbf{R}^{-1}(a_{mn})\mathbf{y}_{mn} \\ &+ \mathbf{y}_{mn}^H\mathbf{R}^{-1}(a_{mn})\mathbf{z}_{mn}\big(\mathbf{z}_{mn}^H\mathbf{R}^{-1}(a_{mn})\mathbf{z}_{mn}\big)^{-1} \\ &\times \mathbf{z}_{mn}^H\mathbf{R}^{-1}(a_{mn})\mathbf{y}_{mn}. \end{aligned} \quad (28)$$

Thus, the MLE of a_{mn} is obtained as

$$\hat{a}_{mn,1} = \arg\max_{a_{mn}} \ f_{\text{CDC}}(a_{mn}), \quad (29)$$

which, similar to (17), requires 1-D search.

Substituting the MLEs under $\mathcal{H}_1$ and $\mathcal{H}_0$, i.e., $\hat{\alpha}$, $\hat{a}_{mn,1}$, and $\hat{a}_{mn,0}$, into the log likelihood ratio (LLR) leads to the coherent detector in clutter (CDC):

$$\begin{aligned} T_{\text{CDC}} =& \sum_{m=1}^{M}\sum_{n=1}^{N}\Big(\ln\frac{|\hat{\mathbf{R}}_0|}{|\hat{\mathbf{R}}_1|} + \mathbf{y}_{mn}^H(\hat{\mathbf{R}}_0^{-1} - \hat{\mathbf{R}}_1^{-1})\mathbf{y}_{mn} \\ &+ \mathbf{y}_{mn}^H\hat{\mathbf{R}}_1^{-1}\mathbf{z}_{mn}(\mathbf{z}_{mn}^H\hat{\mathbf{R}}_1^{-1}\mathbf{z}_{mn})\mathbf{z}_{mn}^H\hat{\mathbf{R}}_1^{-1}\mathbf{y}_{mn}\Big) \underset{\mathcal{H}_0}{\overset{\mathcal{H}_1}{\gtrless}} \gamma_{\text{CDC}}, \end{aligned} \quad (30)$$

where $\hat{\mathbf{R}}_1 = \mathbf{R}(\hat{a}_{mn,1})$. It is seen from (30) that in addition to whitening by covariance matrices $\hat{\mathbf{R}}_1$ and $\hat{\mathbf{R}}_0$, the test statistic

also involves the multiplication by $\mathbf{z}_{mn}^H$, which amounts to filtering by the Doppler matrix $\mathbf{S}_n^H$ and then phase compensation and channel matching by the channel vector $\mathbf{h}_{mn}^H$. Clearly, CDC is a coherent detector.

To avoid 1-D search and reduce the computational complexity, the high CNR approximation, i.e., $a_{mn}\mathbf{\Psi} + \sigma^2\mathbf{I} \approx a_{mn}(\mathbf{\Psi} + \sigma^2\mathbf{I})$, can be employed to convert (29) to

$$\hat{a}_{mn,1} \approx \arg\max_{a_{mn}} \ \widetilde{f}_{\text{CDC}}(a_{mn}), \tag{31}$$

where

$$\widetilde{f}_{\text{CDC}}(a_{mn}) = -\ln\left(a_{mn}^K|\widetilde{\mathbf{R}}|\right) - \frac{1}{a_{mn}}(\mathbf{y}_{mn}^H\widetilde{\mathbf{R}}^{-1}\mathbf{y}_{mn} - \mathbf{y}_{mn}^H\widetilde{\mathbf{R}}^{-1}\mathbf{z}_{mn}(\mathbf{z}_{mn}^H\widetilde{\mathbf{R}}^{-1}\mathbf{z}_{mn})^{-1}\mathbf{z}_{mn}^H\widetilde{\mathbf{R}}^{-1}\mathbf{y}_{mn}). \tag{32}$$

The solution to (31) has a closed-form

$$\hat{a}_{mn,1} \approx \frac{1}{K}\big(\mathbf{y}_{mn}^H\widetilde{\mathbf{R}}^{-1}\mathbf{y}_{mn} - \mathbf{y}_{mn}^H\widetilde{\mathbf{R}}^{-1}\mathbf{z}_{mn}(\mathbf{z}_{mn}^H\widetilde{\mathbf{R}}^{-1}\mathbf{z}_{mn})^{-1}\mathbf{z}_{mn}^H\widetilde{\mathbf{R}}^{-1}\mathbf{y}_{mn}\big). \tag{33}$$

Given the MLEs of the clutter power with high CNR approximation (20) and (33), it is easy to show that the GLRT reduces to

$$T_{\text{CDC-A}} = \prod_{m=1}^{M}\prod_{n=1}^{N}\frac{\hat{a}_{mn,0}}{\hat{a}_{mn,1}} \underset{\mathcal{H}_0}{\overset{\mathcal{H}_1}{\gtrless}} \gamma_{\text{CDC-A}}, \tag{34}$$

which is henceforth referred to as the coherent detector in clutter with approximation (CDC-A).

V. Hybrid detection in clutter

Coherent detection outperforms non-coherent detection at the cost of requiring additional information of the channel including the carrier phase offset between each TX-RX pair. In this section, we consider a hybrid detection approach that obviates the need for the knowledge of the channel vector $\mathbf{h}_{mn}$ and phase synchronization. Instead, it only requires phase coherence of the samples within each CPI to enable Doppler filtering, but the exact phase due to the carrier offset and channel-induced phase shift is not required. Hence, it is a comprise between coherent and non-coherent detection.

Specifically, let $\boldsymbol{\beta}_{mn} \triangleq \alpha\mathbf{h}_{mn}$ which lumps the target RCS and channel vector. A hybrid detector in clutter (HDC) can be obtained by using the GLRT along with the likelihood function $p_1\big(\{\mathbf{y}_{mn}\}|\{\boldsymbol{\beta}_{mn}\},\{a_{mn}\}\big)$ under $\mathcal{H}_1$ parameterized by $\boldsymbol{\beta}_{mn}$ and clutter power a_{mn} and the likelihood function $p_0\big(\{\mathbf{y}_{mn}\}|\{a_{mn}\}\big)$ under $\mathcal{H}_0$:

$$\frac{\max\limits_{\{\boldsymbol{\beta}_{mn}\},\{a_{mn}\}} \ p_1\big(\{\mathbf{y}_{mn}\}|\{\boldsymbol{\beta}_{mn}\},\{a_{mn}\}\big)}{\max\limits_{\{a_{mn}\}} \ p_0\big(\{\mathbf{y}_{mn}\}|\{a_{mn}\}\big)}. \tag{35}$$

Since the MLE of the clutter power under $\mathcal{H}_0$ is given by (17), we only need to solve the estimation problem under $\mathcal{H}_1$. Maximizing the LLF (49) w.r.t. $\boldsymbol{\beta}_{mn}$ (by setting the mean vector to $\boldsymbol{\mu}_{mn} = \mathbf{S}_n\boldsymbol{\beta}_{mn}$) yields its MLE (conditioned on the clutter power a_{mn}) as:

$$\hat{\boldsymbol{\beta}}_{mn} = \big(\mathbf{S}_n^H\mathbf{R}^{-1}(a_{mn})\mathbf{S}_n\big)^{-1}\mathbf{S}_n^H\mathbf{R}^{-1}(a_{mn})\mathbf{y}_{mn}. \tag{36}$$

Substituting the above estimate back into the LLF followed by some simplification, we obtain the MLE of the clutter power as

$$\hat{a}_{mn,1} = \arg\max_{a_{mn}} \ f_{\text{HDC}}(a_{mn}), \tag{37}$$

where

$$f_{\text{HDC}}(a_{mn}) = -\ln|\mathbf{R}(a_{mn})| - \mathbf{y}_{mn}^H\mathbf{R}^{-1}(a_{mn})\mathbf{y}_{mn} + \mathbf{y}_{mn}^H\mathbf{R}^{-1}(a_{mn})\mathbf{S}_n(\mathbf{S}_n^H\mathbf{R}^{-1}(a_{mn})\mathbf{S}_n)^{-1}\mathbf{S}_n^H\mathbf{R}^{-1}(a_{mn})\mathbf{y}_{mn}. \tag{38}$$

Similar to what we have for the NCDC and CDC, the MLE (37) of the clutter power requires 1-D search. After finding all MLEs, substituting them back into the LLR yields the HDC

$$T_{\text{HDC}} = \sum_{m=1}^{M}\sum_{n=1}^{N}\Big(\ln\frac{|\hat{\mathbf{R}}_0|}{|\hat{\mathbf{R}}_1|} + \mathbf{y}_{mn}^H(\hat{\mathbf{R}}_0^{-1} - \hat{\mathbf{R}}_1^{-1})\mathbf{y}_{mn} + \mathbf{y}_{mn}^H\hat{\mathbf{R}}_1^{-1}\mathbf{S}_n(\mathbf{S}_n^H\hat{\mathbf{R}}_1^{-1}\mathbf{S}_n)^{-1}\mathbf{S}_n^H\hat{\mathbf{R}}_1^{-1}\mathbf{y}_{mn}\Big) \underset{\mathcal{H}_0}{\overset{\mathcal{H}_1}{\gtrless}} \gamma_{\text{HDC}}. \tag{39}$$

Compared with the CDC detector (30), HDC (39) retains the whitening and Doppler filtering steps in CDC but dispenses with the phase compensation and channel matching.

The high CNR approximation used earlier can be employed to simplify the optimization problem in (37), which transfers the non-convex cost function into

$$\widetilde{f}_{\text{HDC}}(a_{mn}) = -\ln(a_{mn}^K|\widetilde{\mathbf{R}}|) - \frac{1}{a_{mn}}\big(\mathbf{y}_{mn}^H\widetilde{\mathbf{R}}^{-1}\mathbf{y}_{mn} - \mathbf{y}_{mn}^H\widetilde{\mathbf{R}}^{-1}\mathbf{S}_n(\mathbf{S}_n^H\widetilde{\mathbf{R}}^{-1}\mathbf{S}_n)^{-1}\mathbf{S}_n^H\widetilde{\mathbf{R}}^{-1}\mathbf{y}_{mn}\big). \tag{40}$$

The above cost function can be minimized in closed-form, leading to the following approximate MLE

$$\hat{a}_{mn,1} \approx \frac{1}{K}\Big(\mathbf{y}_{mn}^H\widetilde{\mathbf{R}}^{-1}\mathbf{y}_{mn} - \mathbf{y}_{mn}^H\widetilde{\mathbf{R}}^{-1}\mathbf{S}_n(\mathbf{S}_n^H\widetilde{\mathbf{R}}^{-1}\mathbf{S}_n)^{-1}\mathbf{S}_n^H\widetilde{\mathbf{R}})^{-1}\mathbf{y}_{mn}\Big). \tag{41}$$

Then, after substituting $\hat{a}_{mn,0}$ in (20) and $\hat{a}_{mn,1}$ in (41) back into the likelihood ratio, we obtain a new hybrid detector:

$$T_{\text{HDC-A}} = \prod_{m=1}^{M}\prod_{n=1}^{N}\frac{\hat{a}_{mn,0}}{\hat{a}_{mn,1}} \underset{\mathcal{H}_0}{\overset{\mathcal{H}_1}{\gtrless}} \gamma_{\text{HDC-A}}, \tag{42}$$

which is referred to as the hybrid detection in clutter with approximation (HCD-A) for simplicity. Note that HCD-A shares a similar form as CDC-A (34). The clutter power estimates $\hat{a}_{mn,0}$ and $\hat{a}_{mn,1}$ employed by the two detectors are different.

VI. Simulation results

In this section, simulation results are presented to demonstrate the performance of the proposed detectors, i.e., the NCDC, NCDC-A, and NCDC-CA in Section III, the CDC and CDC-A in Section IV, and the HDC and HDC-A in Section V. These detectors are summarized in Table I. In addition, the NCD, CD, and HD detectors, which were developed in [8] that do not account for the clutter in observations, are included for comparison.

Table I
SUMMARY OF PROPOSED DETECTORS

Detector Name	Summary of Detector
NCDC	Step 1: Compute the MLE $\hat{a}_{mn,0}$ by (17). Step 2: Use $\hat{a}_{mn,0}$ in (14) to form the covariance matrix estimate $\hat{\mathbf{R}}_0$. Step 3: Use $\hat{\mathbf{R}}_0$ and measurements $\mathbf{y}_{mn}$ in (16) to compute the test variable T_{NCDC}.
NCDC-A	Step 1: Compute the covariance matirx $\widetilde{\mathbf{R}}$ by (19). Step 2: Use $\widetilde{\mathbf{R}}$ and measurements $\mathbf{y}_{mn}$ in (22) to compute the test variable $T_{\text{NCDC-A}}$.
NCDC-CA	Step 1: Compute the MLE $\hat{a}_{mn,0}$ by solving the convex problem (24). Step 2: Use $\hat{a}_{mn,0}$ in (14) to form the covariance matrix estimate $\hat{\mathbf{R}}_0$. Step 3: Use $\hat{\mathbf{R}}_0$ and measurements $\mathbf{y}_{mn}$ in (16) to compute the test variable $T_{\text{NCDC-CA}}$.
CDC	Step 1: Compute the MLE $\hat{a}_{mn,0}$ by (17) and the MLE $\hat{a}_{mn,1}$ by (29). Step 2: Use $\hat{a}_{mn,0}$ and $\hat{a}_{mn,1}$ in (14) to form the covariance matrix estimates $\hat{\mathbf{R}}_0$ and $\hat{\mathbf{R}}_1$, respectively. Step 3: Use $\hat{\mathbf{R}}_0$, $\hat{\mathbf{R}}_1$ and measurements $\mathbf{y}_{mn}$ in (30) to compute the test variable T_{CDC}.
CDC-A	Step 1: Compute the MLE $\hat{a}_{mn,0}$ by (20) and the MLE $\hat{a}_{mn,1}$ by (33). Step 2: Use $\hat{a}_{mn,0}$ and $\hat{a}_{mn,1}$ in (34) to compute the test variable $T_{\text{CDC-A}}$.
HDC	Step 1: Compute the MLE $\hat{a}_{mn,0}$ by (17) and the MLE $\hat{a}_{mn,1}$ by (37). Step 2: Use $\hat{a}_{mn,0}$ and $\hat{a}_{mn,1}$ in (14) to form the covariance matrix estimates $\hat{\mathbf{R}}_0$ and $\hat{\mathbf{R}}_1$, respectively. Step 3: Use $\hat{\mathbf{R}}_0$, $\hat{\mathbf{R}}_1$ and measurements $\mathbf{y}_{mn}$ in (39) to compute the test variable T_{HDC}.
HDC-A	Step 1: Compute the MLE $\hat{a}_{mn,0}$ by (20) and the MLE $\hat{a}_{mn,1}$ by (41). Step 2: Use $\hat{a}_{mn,0}$ and $\hat{a}_{mn,1}$ in (42) to compute the test variable $T_{\text{HDC-A}}$.

The signal-to-nosie ratio (SNR) and CNR are defined as

$$\text{SNR} = \sum_{m=1}^{M}\sum_{n=1}^{N}\frac{|\xi_{mn}|^2\mathbb{E}\{|\alpha|^2\}}{\sigma^2}, \tag{43}$$

$$\text{CNR} = \sum_{m=1}^{M}\sum_{n=1}^{N}\sum_{l=1}^{L_{mn}}\frac{|\xi_{mnl}|^2\mathbb{E}\{|\widetilde{\alpha}_{mnl}|^2\}}{\sigma^2}. \tag{44}$$

where the noise variance is chosen as $\sigma^2 = 1$. The target RCS and clutter RCS are randomly generated as $\alpha \sim \mathcal{CN}(0, \sigma_{\text{t}}^2)$ and $\widetilde{\alpha}_{mnl} \sim \mathcal{CN}(0, \sigma_{mnl}^2)$, where σ_{t}^2 and σ_{mnl}^2 are determined based on specific values of SNR and CNR, respectively.

We consider a distributed MIMO radar with $M = 2$ TXs and $N = 1$ RX unless otherwise stated. The propagation delays are $\tau_{11} = 0.1T_p$ and $\tau_{21} = 0.61T_p$, where $T_p = 10^{-5}$ s is the pulse duration. The pulse repetition frequency (PRF) is 500 Hz, the carrier frequency is 3 GHz, the normalized target Doppler frequencies are $f_{11} = 0.3$ and $f_{21} = 0.4$ unless otherwise stated, and the normalized clutter Doppler frequencies $\tilde{f}_{\bar{m}nl}$ are randomly generated with a uniform distribution: $\tilde{f}_{\bar{m}nl} \sim \mathcal{U}\{-\Delta_f, \Delta_f\}$, where $\Delta_f = 0.12$. The number of pulses within a CPI is $K = 10$ unless otherwise stated and the probability of false alarm is $P_f = 10^{-4}$.

Linear frequency modulation waveforms $p_m(t)$ with overlapping instantaneous frequency are employed for testing [46]:

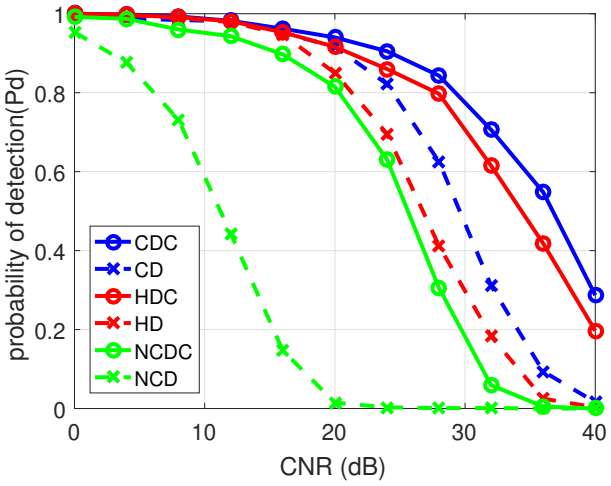

Figure 2. Probability of detection versus CNR when SNR = 18 dB.

$$p_1(t) = \frac{1}{\sqrt{\tau}}e^{\jmath(\pi\beta t^2/T_p + 3\pi\beta t)},\ 0 \le t < T_p, \tag{45}$$

$$p_2(t) = \frac{1}{\sqrt{\tau}}e^{\jmath(-\pi\beta t^2/T_p + 5\pi\beta t)},\ 0 \le t \le T_p, \tag{46}$$

where β denotes the bandwidth of the chirps.

We first consider the performance of the proposed NCDC, CDC, and HDC detectors without any approximations. Fig. 2 shows the probability of detection versus CNR when the SNR = 15 dB. Comparisons between the proposed detectors and their counterparts, namely the NCD, CD, and HD detectors [8] that ignore the clutter, are included. It can be seen that all proposed detectors significantly outperform their counterparts due to the fact that the formers explicitly take into account for the presence of clutter in the observations. Meanwhile, among the three proposed detectors, NCDC has the worst performance, although it does not require any knowledge of the target. CDC achieves the best performance by exploiting the phase and channel information to perform coherent processing. HDC, which is a result of complexity versus performance trade-off, lies between NCDC and CDC. Finally, as CNR increases, the performance of all detectors decreases.

The performance gap in Fig. 2 between the proposed detectors and those of [8] is primarily because the latter neglect clutter, which can significantly impact their performance when the clutter is strong. Let us first consider the NCD detector in [8], which is an energy detector. Specifically, NCD accumulates the energy of the output of all MFs and compares it with a threshold which is determined based on the assumption that the disturbance comprises of only noise (no clutter). NCD does not involve any clutter mitigation; nor does it utilize the target Doppler information for detection. When the observed signal consists of a strong clutter, the clutter dominates the total received energy, in which case whether a target is present or not would result in similar total energy. This creates a difficulty for NCD to distinguish the target-absent state from

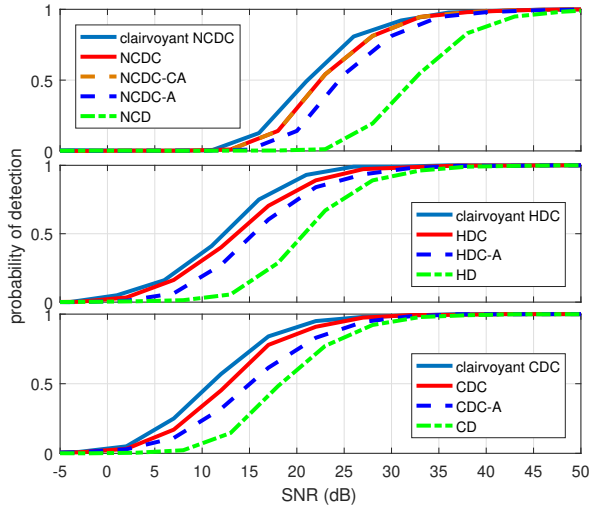

Figure 3. Probability of detection versus SNR when CNR $= 30$ dB.

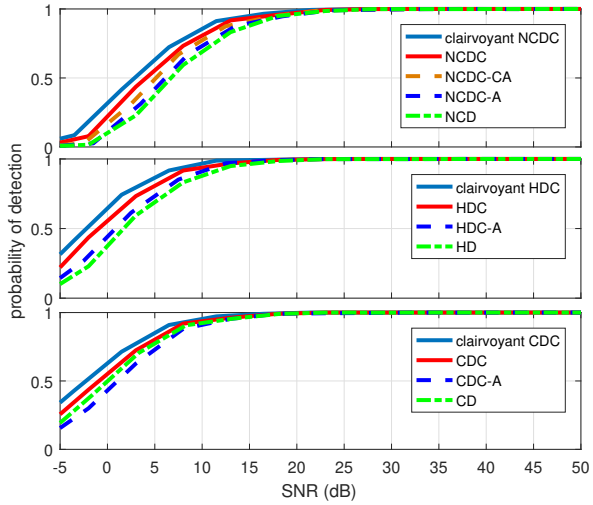

Figure 4. Probability of detection versus SNR when CNR $= 0$ dB.

the target-present state, and hence a substantial performance loss compared with NCDC.

On the other hand, CD and HD experience a smaller performance loss relative to CDC and HDC, respectively. This is because CD and HD do use the target Doppler frequencies for Doppler filtering across slow-time/pulse samples. For example, unlike NCD which indiscriminately uses the energy of the entire Doppler band, HCD involves a projection which integrates the target signal energy in the target Doppler frequency bands for detection. When the clutter and target occupy non-overlapping Doppler frequency bands, the Doppler filtering also partially rejects clutter by filtering out the clutter outside the target bands. This is why CD and HD show a smaller performance loss in the presence of clutter. Nevertheless, when the clutter is strong, there is non-negligible clutter energy in the target bandwidth due to leakage, which causes CD and HCD to underperform their counterparts in Fig. 2.

We next evaluate the performance of the proposed detectors with approximations. For benchmarking, we also include the clairvoyant detectors for each category which assume the

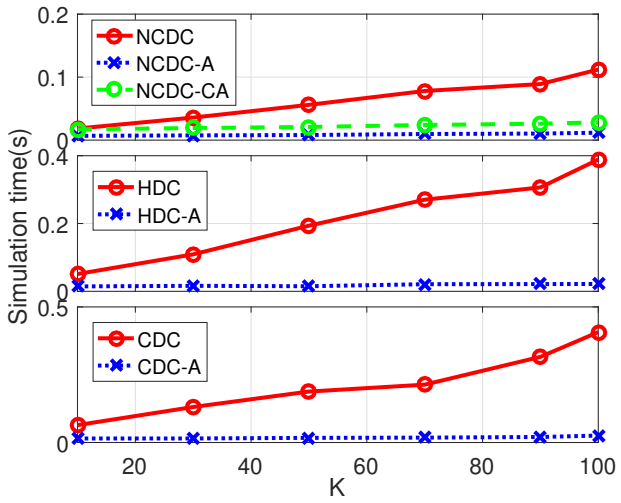

Figure 5. Simulation time versus K the number of pulses within a CPI, when CNR $= 30$ dB and SNR $= 18$ dB.

knowledge of the unknown parameters. Fig. 3 and 4 show the probability of detection for the detectors with/without approximation against various SNR under both a high CNR scenario with CNR $= 30$ dB, and respectively, a low CNR case with CNR $= 0$ dB. It can be seen from Fig. 3 that when clutter is strong, the proposed detectors with or without approximation, i.e., NCDC/NCDC-A/NCDC-CA, HCDC/HCDC-A, and CDC/CDC-A, significantly outperform their counterparts NCD, HD, and CD. This is because in this case, the clutter has a strong impact on the detection performance. It is also seen that convex approximation based NCDC-CA, which surpasses the high CNR approximation based NCD-A, achieves a performance nearly identical to that of NCDC. Meanwhile, at CNR $= 0$ dB, the clutter reduces to the noise level. The performance gaps between the corresponding detectors as shown in Fig. 4 become considerably smaller. Hence, the original NCD, HD and CD might be opted for to seek lower computational complexity when the clutter becomes negligible. It is also seen that while the clairvoyant detectors have the best performance, the proposed NCDC, CDC, and HDC only exhibit a small performance loss compared with clairvoyant counterpart.

Next, we compare the computational complexities of the proposed detectors with and without approximation. Specifically, Fig. 5 shows the simulation time of each detector in one Monte Carlo trial versus K the number of pulses within a CPI. On one hand, it can be observed that the simulation time of the proposed detectors without approximation increases substantially as K increases. This is because these detectors involve non-convex estimation which requires brute force search. As K increases, the observation size increases, which results in larger vectors/matrices and in turn, higher computation complexity. On the other hand, high CNR approximation, which leads to closed-form estimation solutions, reduces significantly the complexity and simulation time. NCDC-CA with convex relaxation has a higher complexity than NCDC-A since, while it transfers the original non-convex problem into a convex one, the latter does not a closed-form solution. It also requires several iterations for the solution to converge.

Finally, we examine the impact of the target Doppler frequencies relative to the clutter Doppler bandwidth (BW) $[-0.12, 0.12]$. For comparison, we include the detectors under study with $M = 2$ and $M = 1$, respectively, the latter corresponding to a conventional system with a single transmit antenna. The conventional system is formed by using the first antenna of the MIMO system, but transmits at twice the power level so that the two systems have an identical total transmit power for fair comparison. We consider three cases for the normalized target Doppler frequencies:

- **Case 1**: $f_{11} = 0.3$ and $f_{21} = 0.4$ for $M = 2$; $f_{11} = 0.3$ for $M = 1$, where the target Doppler frequencies are all far from the clutter Doppler BW.
- **Case 2**: $f_{11} = 0.13$ and $f_{21} = 0.4$ for $M = 2$; $f_{11} = 0.13$ for $M = 1$, where the MIMO system has one target Doppler frequency that is far from from the clutter BW.
- **Case 3**: $f_{11} = 0.13$ and $f_{21} = 0.14$ for $M = 2$; $f_{11} = 0.13$ for $M = 1$, where the target Doppler frequencies are all near the clutter Doppler BW.

The results of the proposed detectors with approximations are omitted to better illustrate the impact of Doppler frequencies. Fig. 6 shows the performance of the non-coherent detectors when CNR $= 30$ dB. It can be seen from Fig. 6 that the performance of the proposed NCDC decreases considerably from Case 1 to Case 3. This is because when the target Doppler frequencies are near the clutter BW, it becomes harder to separate the target from clutter. It is also seen that the MIMO system with $M = 2$ outperforms the conventional system with $M = 1$ in all 3 cases. Specifically, in Case 2 the conventional system degrades significantly relative to Case 1 because its target Doppler frequency is near the clutter BW, whereas the MIMO system excels as among its two observed target Doppler frequencies, one is far from the clutter BW. This result signifies the benefit of diversity of the MIMO system, which observes the target from different aspect angles, leading to diverse target Doppler frequencies. As long as one target Doppler frequency is not near the clutter Doppler BW, the system is able to separate the target from clutter. Meanwhile, if all observed target Doppler frequencies are near the clutter BW, as in Case 3, the MIMO system loses much of its benefit of diversity. Similar relations can be observed in Figs. 7 and 8 for the hybrid and coherent detectors. One notable difference in these figures is that the original HD and CD also deteriorate substantially from Case 1, Case 2, to Case 3. That is because, as discussed earlier, these detectors implicitly perform some clutter rejection through Doppler filtering. When the target and clutter Doppler frequencies become overlapping as in Case 2 and Case 3, the Doppler filtering employed by these detectors pass not only the target signal but also a significant amount of clutter, causing their performance degradation.

VII. Conclusions

We examined target detection using distributed MIMO radar with non-orthogonal waveforms in cluttered environments. Our main contributions comprise a general signal model for the considered problem and three families of detectors, including the non-coherent NCDC, NCDC-A, and NCDC-CA,

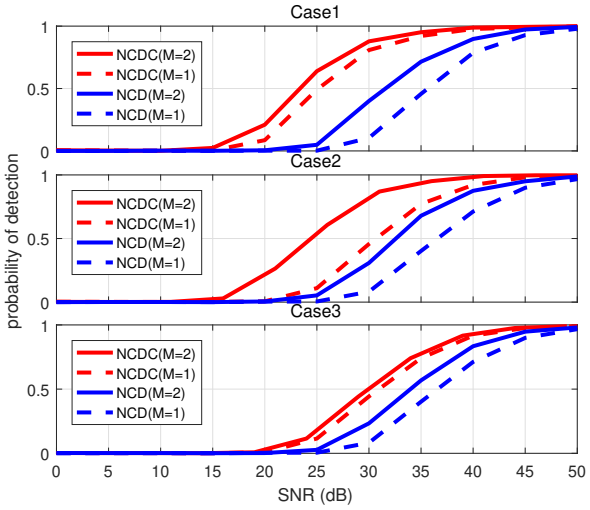

Figure 6. Probability of detection versus SNR with non-coherent detection with a MIMO ($M = 2$) and a conventional ($M = 1$) system when CNR $= 30$ dB.

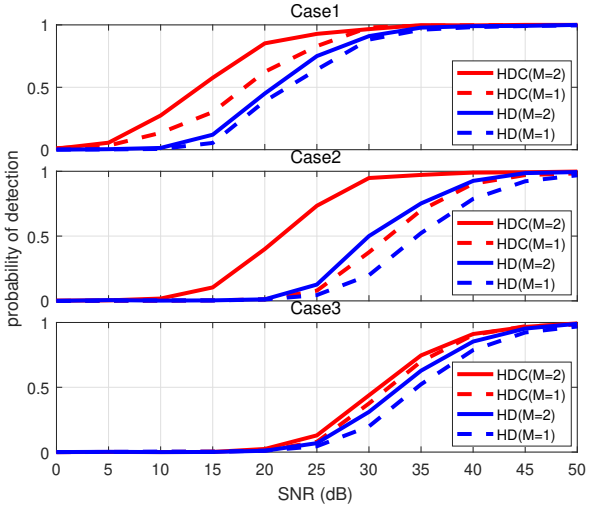

Figure 7. Probability of detection versus SNR with hybrid detection with a MIMO ($M = 2$) and a conventional ($M = 1$) system when CNR $= 30$ dB.

the coherent CDC and CDC-A, as well as the hybrid HDC and HDC-A. Our results indicate that the proposed detectors significantly surpass their earlier counterparts in cluttered environments. The proposed detectors with approximation can greatly reduce the computational complexity with only a minor performance loss. In addition, these MIMO detectors exhibit an improved target detection ability compared with conventional single-antenna based schemes due to spatial diversity.

Appendix I
ML Estimation Derivation for NCDC

Under $\mathcal{H}_0$, the unknown parameters are $\{a_{mn}\}$. The LLF is given by

$$\ln p_0\big(\{\mathbf{y}_{mn}\}|\{a_{mn}\}\big) = -\sum_{m=1}^{M}\sum_{n=1}^{N}\Big[\ln|\mathbf{R}(a_{mn})| + \mathbf{y}_{mn}^H\mathbf{R}^{-1}(a_{mn})\mathbf{y}_{mn}\Big]. \quad (47)$$

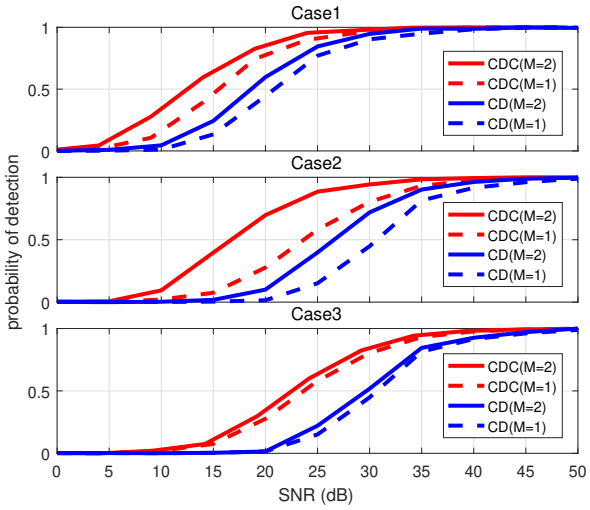

Figure 8. Probability of detection versus SNR with coherent detection with a MIMO ($M = 2$) and a conventional ($M = 1$) system when CNR $= 30$ dB.

Then, the MLE of a_{mn} under $\mathcal{H}_0$ can be obtained by solving the following optimization problem:

$$\min_{a_{mn}} \quad \ln|\mathbf{R}(a_{mn})| + \mathbf{y}_{mn}^H \mathbf{R}^{-1}(a_{mn})\mathbf{y}_{mn} \ . \tag{48}$$

Under $\mathcal{H}_1$, the unknown parameters are $\{\boldsymbol{\mu}_{mn}\}$ and $\{a_{mn}\}$. The LLF is given by

$$\ln p_1\big(\{\mathbf{y}_{mn}\}|\{\boldsymbol{\mu}_{mn}\},\{a_{mn}\}\big) = -\sum_{m=1}^{M}\sum_{n=1}^{N}\Big[\ln|\mathbf{R}(a_{mn})| + (\mathbf{y}_{mn}-\boldsymbol{\mu}_{mn})^H\mathbf{R}^{-1}(a_{mn})(\mathbf{y}_{mn}-\boldsymbol{\mu}_{mn})\Big]. \tag{49}$$

The MLE of $\boldsymbol{\mu}_{mn}$ is obtained by taking the derivative of the LLF in (49) w.r.t. $\boldsymbol{\mu}_{mn}$, and setting it to zero, which yields:

$$\hat{\boldsymbol{\mu}}_{mn} = \mathbf{y}_{mn}. \tag{50}$$

Substituting the above MLE back to (49), the LLF reduces to

$$\ln p_1\big(\{\mathbf{y}_{mn}\}|\{a_{mn}\}\big) = -\sum_{m=1}^{M}\sum_{n=1}^{N}\ln|\mathbf{R}(a_{mn})|. \tag{51}$$

which is independent of the observations $\mathbf{y}_{mn}$, and so is the MLE of a_{mn}.

Since the LLF under $\mathcal{H}_1$ with the parameters replaced by their MLEs becomes independent of the observations, the GLRT only depends on the likelihood function under $\mathcal{H}_0$. This leads to the NCDC detector given by (16), where the test statistic is essentially the negative LLF under $\mathcal{H}_0$.

REFERENCES

[1] A. M. Haimovich, R. S. Blum, and L. J. Cimini, "MIMO radar with widely separated antennas," *IEEE Signal Processing Magazine*, vol. 25, no. 1, pp. 116–129, 2007.

[2] E. Fishler, A. Haimovich, R. S. Blum, L. J. Cimini, D. Chizhik, and R. A. Valenzuela, "Spatial diversity in radarsmodels and detection performance," *IEEE Transactions on Signal Processing*, vol. 54, no. 3, pp. 823–838, 2006.

[3] Q. He and R. S. Blum, "Diversity gain for MIMO Neyman–Pearson signal detection," *IEEE Transactions on Signal Processing*, vol. 59, no. 3, pp. 869–881, 2010.

[4] N. H. Lehmann, E. Fishler, A. M. Haimovich, R. S. Blum, D. Chizhik, L. J. Cimini, and R. A. Valenzuela, "Evaluation of transmit diversity in MIMO-radar direction finding," *IEEE transactions on Signal Processing*, vol. 55, no. 5, pp. 2215–2225, 2007.

[5] A. Tajer, G. H. Jajamovich, X. Wang, and G. V. Moustakides, "Optimal joint target detection and parameter estimation by MIMO radar," *IEEE Journal of Selected Topics in Signal Processing*, vol. 4, no. 1, pp. 127–145, 2010.

[6] J. Liu, Z.-J. Zhang, Y. Cao, and S. Yang, "A closed-form expression for false alarm rate of adaptive MIMO-glrt detector with distributed MIMO radar," *Signal Processing*, vol. 93, no. 9, pp. 2771–2776, 2013.

[7] W. Yi, T. Zhou, Y. Ai, and R. S. Blum, "Suboptimal low complexity joint multi-target detection and localization for non-coherent MIMO radar with widely separated antennas," *IEEE Transactions on Signal Processing*, vol. 68, pp. 901–916, 2020.

[8] H. Li, F. Wang, C. Zeng, and M. A. Govoni, "Signal detection in distributed MIMO radar with non-orthogonal waveforms and sync errors," *IEEE Transactions on Signal Processing*, vol. 69, pp. 3671–3684, 2021.

[9] C. Zeng, F. Wang, H. Li, and M. A. Govoni, "New coherent and hybrid detectors for distributed mimo radar with synchronization errors," in *2021 IEEE Radar Conference (RadarConf21)*. IEEE, 2021, pp. 1–5.

[10] S. Gogineni and A. Nehorai, "Target estimation using sparse modeling for distributed MIMO radar," *IEEE Transactions on Signal Processing*, vol. 59, no. 11, pp. 5315–5325, 2011.

[11] M. Einemo and H. C. So, "Weighted least squares algorithm for target localization in distributed MIMO radar," *Signal Processing*, vol. 115, pp. 144–150, 2015.

[12] J. Liang, C. S. Leung, and H. C. So, "Lagrange programming neural network approach for target localization in distributed MIMO radar," *IEEE Transactions on Signal Processing*, vol. 64, no. 6, pp. 1574–1585, 2015.

[13] M. M. Naghsh, M. Modarres-Hashemi, M. A. Kerahroodi, and E. H. M. Alian, "An information theoretic approach to robust constrained code design for MIMO radars," *IEEE Transactions on Signal Processing*, vol. 65, no. 14, pp. 3647–3661, 2017.

[14] S. G. Dontamsetti and R. V. R. Kumar, "A distributed MIMO radar with joint optimal transmit and receive signal combining," *IEEE Transactions on Aerospace and Electronic Systems*, vol. 57, no. 1, pp. 623–635, 2020.

[15] H. Godrich, A. P. Petropulu, and H. V. Poor, "Power allocation strategies for target localization in distributed multiple-radar architectures," *IEEE Transactions on Signal Processing*, vol. 59, no. 7, pp. 3226–3240, 2011.

[16] M. Radmard, M. M. Chitgarha, M. N. Majd, and M. M. Nayebi, "Antenna placement and power allocation optimization in MIMO detection," *IEEE Transactions on Aerospace and Electronic Systems*, vol. 50, no. 2, pp. 1468–1478, 2014.

[17] Q. He, R. S. Blum, H. Godrich, and A. M. Haimovich, "Target velocity estimation and antenna placement for MIMO radar with widely separated antennas," *IEEE Journal of Selected Topics in Signal Processing*, vol. 4, no. 1, pp. 79–100, 2010.

[18] M. Sadeghi, F. Behnia, R. Amiri, and A. Farina, "Target localization geometry gain in distributed MIMO radar," *IEEE Transactions on Signal Processing*, vol. 69, pp. 1642–1652, 2021.

[19] Q. He and R. S. Blum, "Cramer–rao bound for MIMO radar target localization with phase errors," *IEEE Signal Processing Letters*, vol. 17, no. 1, pp. 83–86, 2009.

[20] Q. Hu, H. Su, S. Zhou, Z. Liu, and J. Liu, "Target detection in distributed MIMO radar with registration errors," *IEEE Transactions on Aerospace and Electronic Systems*, vol. 52, no. 1, pp. 438–450, 2016.

[21] J. Liu, K. V. Mishra, and M. Saquib, "Co-designing statistical MIMO radar and in-band full-duplex multi-user MIMO communications," *arXiv preprint arXiv:2006.14774*, 2020.

[22] A. Ahmed, Y. D. Zhang, and B. Himed, "Distributed dual-function radar-communication MIMO system with optimized resource allocation," in *2019 IEEE Radar Conference (RadarConf)*. IEEE, 2019, pp. 1–5.

[23] Y. I. Abramovich and G. J. Frazer, "Bounds on the volume and height distributions for the MIMO radar ambiguity function," *IEEE Signal Processing Letters*, vol. 15, pp. 505–508, 2008.

[24] G. San Antonio, D. R. Fuhrmann, and F. C. Robey, "MIMO radar ambiguity functions," *IEEE Journal of Selected Topics in Signal Processing*, vol. 1, no. 1, pp. 167–177, 2007.

[25] F. Daum and J. Huang, "MIMO radar: Snake oil or good idea?" *IEEE Aerospace and Electronic Systems Magazine*, vol. 24, no. 5, pp. 8–12, 2009.

[26] B. Liao, "Fast angle estimation for MIMO radar with nonorthogonal waveforms," *IEEE Transactions on Aerospace and Electronic Systems*, vol. 54, no. 4, pp. 2091–2096, 2018.

[27] N.-J. Ruan, F.-q. Wen, L. Ai, and K. Xie, "A PARAFAC decomposition algorithm for DOA estimation in colocated MIMO radar with imperfect waveforms," *IEEE Access*, vol. 7, pp. 14 680–14 688, 2019.

[28] F. Wen, "Computationally efficient DOA estimation algorithm for MIMO radar with imperfect waveforms," *IEEE Communications Letters*, vol. 23, no. 6, pp. 1037–1040, 2019.

[29] M. Akçakaya and A. Nehorai, "MIMO radar sensitivity analysis for target detection," *IEEE Transactions on Signal Processing*, vol. 59, no. 7, pp. 3241–3250, 2011.

[30] P. Wang and H. Li, "Target detection with imperfect waveform separation in distributed MIMO radar," *IEEE Transactions on Signal Processing*, vol. 68, pp. 793–807, 2020.

[31] H. Li, Z. Wang, J. Liu, and B. Himed, "Moving target detection in distributed MIMO radar on moving platforms," *IEEE Journal of Selected Topics in Signal Processing*, vol. 9, no. 8, pp. 1524–1535, 2015.

[32] P. Wang, H. Li, and B. Himed, "Moving target detection using distributed MIMO radar in clutter with nonhomogeneous power," *IEEE Transactions on Signal Processing*, vol. 59, no. 10, pp. 4809–4820, 2011.

[33] A. Zaimbashi, "Invariant subspace detector in distributed multiple-input multiple output radar: Geometry gain helps improving moving target detection," *IET Radar, Sonar & Navigation*, vol. 10, no. 5, pp. 923–934, 2016.

[34] P. Chen, L. Zheng, X. Wang, H. Li, and L. Wu, "Moving target detection using colocated MIMO radar on multiple distributed moving platforms," *IEEE Transactions on Signal Processing*, vol. 65, no. 17, pp. 4670–4683, 2017.

[35] A. Hassanien, B. Himed, and B. D. Rigling, "Robust moving target detection for distributed MIMO radar in non-homogeneous clutter," in *2019 International Radar Conference (RADAR)*. IEEE, 2019, pp. 1–6.

[36] A. Hassanien and B. Himed, "Moving target detection for distributed MIMO radar under clutter model mismatch," in *2020 54th Asilomar Conference on Signals, Systems, and Computers*. IEEE, 2020, pp. 1568–1573.

[37] P. Wang, H. Li, and B. Himed, "A parametric moving target detector for distributed MIMO radar in non-homogeneous environment," *IEEE Transactions on Signal Processing*, vol. 61, no. 9, pp. 2282–2294, 2013.

[38] M. Akcakaya and A. Nehorai, "Adaptive MIMO radar design and detection in compound-Gaussian clutter," *IEEE Transactions on Aerospace and Electronic Systems*, vol. 47, no. 3, pp. 2200–2207, 2011.

[39] N. Li, G. Cui, L. Kong, and X. Yang, "Rao and Wald tests design of multiple-input multiple-output radar in compound-gaussian clutter," *IET Radar, Sonar & Navigation*, vol. 6, no. 8, pp. 729–738, 2012.

[40] G. Cui, L. Kong, X. Yang, and J. Yang, "Distributed target detection with polarimetric MIMO radar in compound-Gaussian clutter," *Digital Signal Processing*, vol. 22, no. 3, pp. 430–438, 2012.

[41] T. Zhang, G. Cui, L. Kong, and X. Yang, "Adaptive Bayesian detection using MIMO radar in spatially heterogeneous clutter," *IEEE Signal Processing Letters*, vol. 20, no. 6, pp. 547–550, 2013.

[42] Y. Gao, H. Li, and B. Himed, "Knowledge-aided range-spread target detection for distributed MIMO radar in nonhomogeneous environments," *IEEE Transactions on Signal Processing*, vol. 65, no. 3, pp. 617–627, 2016.

[43] J. Ward, "Space-time adaptive processing for airborne radar," Lincoln Laboratory, MIT, Technical Report 1015, December 1994.

[44] Y. Sun, P. Babu, and D. P. Palomar, "Majorization-minimization algorithms in signal processing, communications, and machine learning," *IEEE Transactions on Signal Processing*, vol. 65, no. 3, pp. 794–816, 2016.

[45] M. A. Richards, *Fundamentals of Radar Signal Processing*. McGraw-Hill Education, 2014.

[46] F. Wang, C. Zeng, H. Li, and M. A. Govoni, "Detection performance of distributed MIMO radar with asynchronous propagation and timing/phase errors," in *2020 IEEE International Radar Conference (RADAR)*. IEEE, 2020, pp. 13–18.

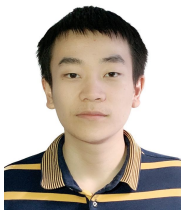

Cengcang Zeng received the B.S. degree from Nanjing University of Aeronautics and Astronautics, Nanjing, China in 2016 and the M.S. degree from Stevens Institute of Technology, Hoboken, NJ, USA in 2018, both in electrical engineering. He is currently pursuing the Ph.D. degree in electrical engineering at Stevens Institute of Technology, Hoboken, NJ, USA. He has been a Research Assistant in the Department of Electrical and Computer Engineering, Stevens Institute of Technology, Hoboken, NJ, USA, since 2020. His research interests include statistical signal processing and convex optimization, focusing on radar signal processing.

Fangzhou Wang (M'22) received the B.S. and M.S. degrees from Beijing Institute of Technology, Beijing, China in 2012 and 2015, respectively, and the Ph.D. degree from Stevens Institute of Technology, Hoboken, NJ, in 2022, all in electrical engineering. He is currently a postdoctoral scholar with the Department of Electrical Engineering and Computer Science at University of California Irvine, CA. His research interests include statistical signal processing and convex optimization, with emphasis on wireless communications and radar signal processing.

Dr. Wang received the Outstanding Ph.D. Dissertation Award in Electrical Engineering in 2022, the Paul Kaplan Award for Distinguished Doctoral Work in 2022, and the Outstanding Research Assistant Award in 2018, all from Stevens Institute of Technology. He is a frequent reviewer for *IEEE Transactions on Signal Processing*, *IEEE Journal of Selected Topics in Signal Processing*, *IEEE Transactions on Aerospace and Electronics Systems*, *IEEE Transactions on Vehicular Technology*, *IEEE Transactions on Wireless Communications*, *IEEE Transactions on Communications*, *IEEE Signal Processing Letters*, and *IEEE Wireless Communications Letter*.

Hongbin Li (M'99-SM'08-F'19) received the B.S. and M.S. degrees from the University of Electronic Science and Technology of China, in 1991 and 1994, respectively, and the Ph.D. degree from the University of Florida, Gainesville, FL, in 1999, all in electrical engineering.

From July 1996 to May 1999, he was a Research Assistant in the Department of Electrical and Computer Engineering at the University of Florida. Since July 1999, he has been with the Department of Electrical and Computer Engineering, Stevens Institute of Technology, Hoboken, NJ, where he is currently the Charles and Rosanna Batchelor Memorial Chair Professor. He was a Summer Visiting Faculty Member at the Air Force Research Laboratory in the summers of 2003, 2004 and 2009. His general research interests include statistical signal processing, wireless communications, and radars.

Dr. Li received the IEEE Jack Neubauer Memorial Award in 2013 from the IEEE Vehicular Technology Society, Outstanding Paper Award from the IEEE AFICON Conference in 2011, Provost's Award for Research Excellence in 2019, Harvey N. Davis Teaching Award in 2003, and Jess H. Davis Memorial Research Award in 2001 from Stevens Institute of Technology, and Sigma Xi Graduate Research Award from the University of Florida in 1999. He has been a member of the IEEE SPS Signal Processing Theory and Methods Technical Committee (TC) and the IEEE SPS Sensor Array and Multichannel TC, an Associate Editor for *Signal Processing* (Elsevier), *IEEE Transactions on Signal Processing*, *IEEE Signal Processing Letters*, and *IEEE Transactions on Wireless Communications*, as well as a Guest Editor for *IEEE Journal of Selected Topics in Signal Processing* and *EURASIP Journal on Applied Signal Processing*. He has been involved in various conference organization activities, including serving as a General Co-Chair for the 7th IEEE Sensor Array and Multichannel Signal Processing (SAM) Workshop, Hoboken, NJ, June 17-20, 2012. Dr. Li is a member of Tau Beta Pi and Phi Kappa Phi.

Mark A. Govoni (M'02-SM'12) received the B.S.E. and M.S. degrees from Arizona State University, Tempe, AZ, USA, in 2000 and 2001, respectively, and the Ph.D. from the Stevens Institute of Technology, Hoboken, NJ, USA in 2011. He has authored or coauthored more than 100 technical publications/documents including 1 book chapter and holds 12 patents. His research interests include signal processing, electromagnetic phenomenology, waveform design, and radar system optimization techniques.